

Bifurcation Structure of a Three-Species Food Chain Model

KEVIN McCANN AND PETER YODZIS

Department of Zoology, University of Guelph, Guelph, Ontario

Received June 1, 1993

A three-species food chain model utilizing type II functional responses and allometric relationships is analyzed mathematically. A reduction of the two-dimensional nullsurfaces to a set of one-dimensional curves allows for an intuitive understanding of the equilibria structure. With the reduction in hand, we then perform a local bifurcation analysis around an organizing center and categorize the entire parameter space into twelve different regions of dynamic behaviour. These regions in parameter space are characterized by an extremely rich set of dynamical behaviours, including multiple domains of attraction, quasi-periodicity, chaos, homoclinic events, and transient chaos. From this mathematical analysis it is possible to qualify the type of population dynamics under any given parameter set. © 1995 Academic Press, Inc.

I. INTRODUCTION

Since the time of Lotka (1925) and Volterra (1926), the use of ordinary differential equations in consumer-resource population modelling has been a source of great contention. These simple and general models have offered insights into community structure and other population phenomena. However, biologists have criticized the approach for its lack of biological rigor. Parameters are abstractly defined and do little to bridge the gap between theorists and empiricists. Recently, Yodzis and Innes (1992) have begun to cross this void by clarifying the derivation of these parameters using well-known allometric and energetic relations. We will extend their model from a two-dimensional context to the dynamically more interesting three-dimensional simple food chain model. The ability to utilize body size relationships among consumers and resources in parameter estimation enables this increase in dimension—and the corresponding increase in parameters—to be executed judiciously. Any jump in dimension within a modelling context is dangerous as informational error may be multiplied. With the aid of Yodzis and Innes' estimation technique we now have a tool with which to measure the biological "plausibility" of any parametric

setting by calculating consumer-resource mass ratios and comparing them to empirically derived relationships.

Research on three-dimensional simple food chains has focused primarily on persistence (Rosenzweig, 1973; Freedman and Waltman, 1977; Freedman and So, 1985) or strange phase space dynamics in a restricted area of parameter space (Hastings and Powell, 1991). We will differ from these approaches in two major ways. One, we will attempt to qualify the global phase space behaviour over the entire region in parameter space. Two, we will construct a model that is derived from allometric relationships such that we are able to assess the biological plausibility of any parameter setting.

The mathematical analysis will start by creating an intuitive feel for the equilibrium structure of the model. This will be accomplished by reducing the nullsurfaces to diagrams in two-dimensional space with tolerable loss of information. The reduced nullsurface diagram acts as a powerful tool for interpreting effects of the various parameters on the equilibrium structure, stability and local bifurcation behaviour. After finding the local bifurcations we then perform a bifurcation analysis around an organizing center (Thom, 1975) and qualify behaviour within defined regions of the unfolding parameters under consideration. Klebanoff and Hastings (1994) have performed a related bifurcation analysis. Our method of bifurcation analysis makes possible a predictive measure for phase space dynamics at any point in parameter space. The analysis will unfold a complex global structure including multiple equilibria, multiple basins of attraction, chaos, and chaotic transients. Furthermore, possible routes to chaos are explored and the existence of global bifurcations is posed as likely.

Our analysis is undertaken with the primary motivation of gaining insight into trophodynamic behaviour of three-dimensional systems. Population models have traditionally been concerned primarily with local stability structure in qualifying dynamic behaviour. This paper emphasizes a more global perspective and finds that simple local structures can have a relatively complicated set of global phase spaces.

II. THE MODEL

The model used here is a simple three-species food chain model analogous to the bioenergetic consumer-resource model derived by Yodzis and Innes (1992). The state variables R , C , and P represent resource, intermediate consumer, and top predator, respectively. We allow for the resource population to grow logistically without consumers present and consumption (for both C and P) is at a rate proportional to a Holling type II functional response without predator interference. Utilizing the above

assumptions and Yodzis and Innes' (1992) allometric reasoning we get the system

$$\begin{aligned}\frac{dR}{dt} &= r \left(1 - \frac{R}{K}\right) - x'_C y_C \frac{CR}{f_C(1 - \delta_C)(R + R_0)} \\ \frac{dC}{dt} &= -x'_C \left(1 - y_C \frac{R}{R + R_0}\right) - x'_P y_P \frac{PC}{f_P(1 - \delta_P)(C + C_0)} \\ \frac{dP}{dt} &= -x'_P P \left(1 - y_P \frac{C}{C + C_0}\right),\end{aligned}\quad (1)$$

where r is the per capita rate of increase of R , K is the carrying capacity of R , δ_i is the fraction of ingested energy lost to egestion and excretion by species i , R_0 and C_0 are the half-saturation densities of resources R and C by consumers C and P , respectively, f represents certain fractional properties of specific populations i , and x_C, x_P, y_C, y_P , are functions of adult body masses of R , C , and P (m_R, m_C, m_P respectively) shown below:

$$x_C = a_T (m_R/m_C)^{0.25} / [f_R a_R] \quad (2)$$

$$x_P = b_T (m_R/m_P)^{0.25} / [f_R a_R] \quad (3)$$

$$y_C = f_C a_J / a_T \quad (4)$$

$$y_P = f_P b_J / b_T. \quad (5)$$

Parameter values for the constants a_R, a_T, a_J, b_T, b_J , and δ_i empirically derived for various metabolic types of animals are shown in Table I (taken from Yodzis and Innes, 1992). The parameters y_C (y_P) have upper bounds, $y_{\max i}$, given in Table I.

With the aid of some transformations we can reduce the number of parameters from twelve to six. By performing the transformations

$$R \rightarrow \frac{R}{K} \quad (6)$$

$$C \rightarrow \frac{C}{K f_C (1 - \delta_C)} \quad (7)$$

$$P \rightarrow \frac{P}{K f_C f_P (1 - \delta_C) (1 - \delta_P)} \quad (8)$$

$$t \rightarrow rt, \quad (9)$$

TABLE I
Empirically Determined Parameter Values

Parameter	Carnivore	Herbivore	Endotherm	Vertebrate ectotherm	Invertebrate	Phyto- plankton
δ_1	0.15	0.55
a_T or b_T	54.9	2.3	0.5	...
a_J or b_J		...	89.2	8.9	9.7	
a_r	34.3	6.6	0.3	0.4
y_{\max}	...		6	3.9	19.4	

Note. Table values and derivations are from Yodzis and Innes (1992). The quantity δ is the fraction of ingested energy lost to feces and urine; a_J , a_T (units $\text{kg} [\text{kg yr}]^{-1} \text{kg}^{0.25}$) are the coefficients determined from allometric relationships for the consumer C , while b_J and b_T (units $\text{kg} [\text{kg yr}]^{-1} \text{kg}^{0.25}$) are the same coefficients determined from allometric relationships for the top predator P ; y_{\max} (a_J/a_T or b_J/b_T) is the maximum value that parameters y_C (y_P) can attain.

system (1) can be reduced to

$$\begin{aligned} \frac{dR}{dt} &= F_R = R(1 - R) - x_C y_C \frac{CR}{R + R_0} \\ \frac{dC}{dt} &= F_C = -x_C C \left(1 - y_C \frac{R}{R + R_0} \right) - x_P y_P \frac{PC}{C + C_0} \\ \frac{dP}{dt} &= F_P = -x_P P \left(1 - y_P \frac{C}{C + C_0} \right), \end{aligned} \quad (10)$$

where our six non-dimensional parameters can be defined in terms of the original parameters as seen in Table II and all are nonnegative.

TABLE II
Non-dimensional Parameters in terms of Dimensional Parameters

Non-dimensional parameters	Dimensional parameters
x_C	x'_C/r
x_P	x'_P/r
R_0	R'_0/K
C_0	$C_0/[Kf_{ec}(1 - d_e)]$
y_C	...
y_P	...

Note. y_C and y_P are already non-dimensional parameters in system (10).

III. SOME GEOMETRY AND PROPERTIES OF THE MODEL

Two-dimensional models in ecology have often exploited the use of zero isoclines or nullsurfaces in developing an understanding for the dynamic behaviour of the system. Three-dimensional nullsurfaces suffer in that they become a complex of tangled surfaces and provide little if any intuitive insight into the dynamical nature of the model. For example the nullsurfaces of system (10) can be generated by equating right-hand sides of (10) to zero. When this is done we generate the three surfaces,

$$C = [-R^2 + (1 - R_0)R + R_0]/(x_C y_C), \quad (11)$$

$$P = x_C(1 - y_C R/(R + R_0))(C + C_0)/(x_P y_P), \quad (12)$$

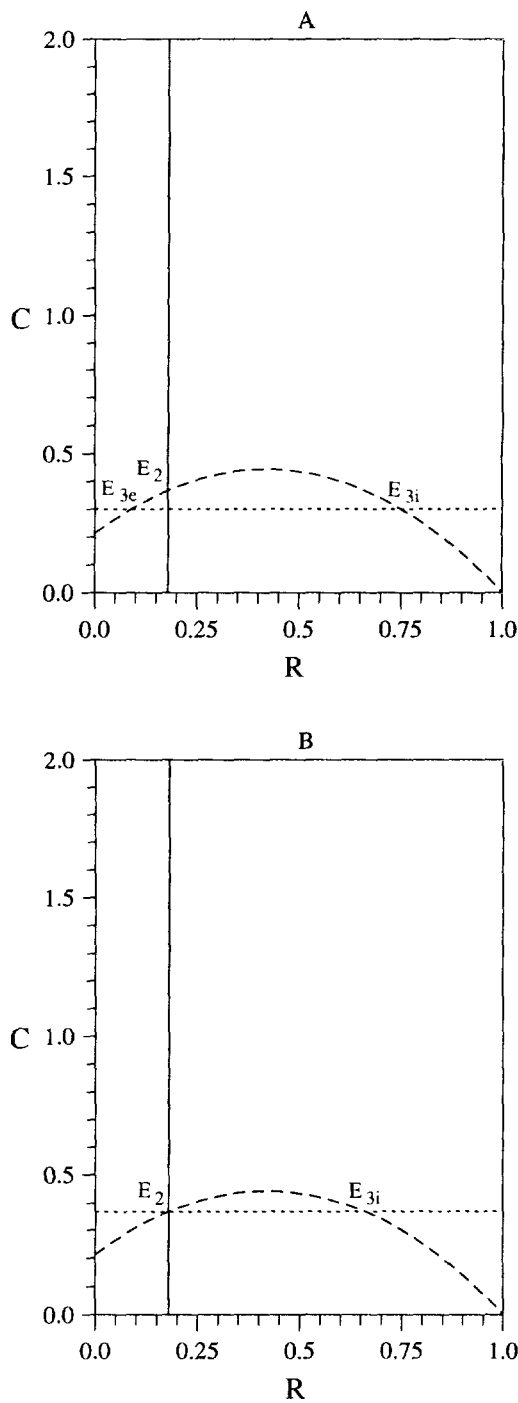
$$C = C_0/(y_P - 1), \quad (13)$$

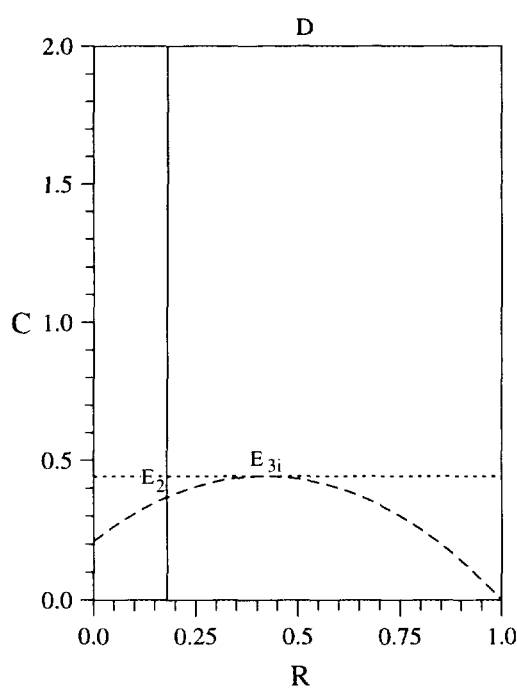
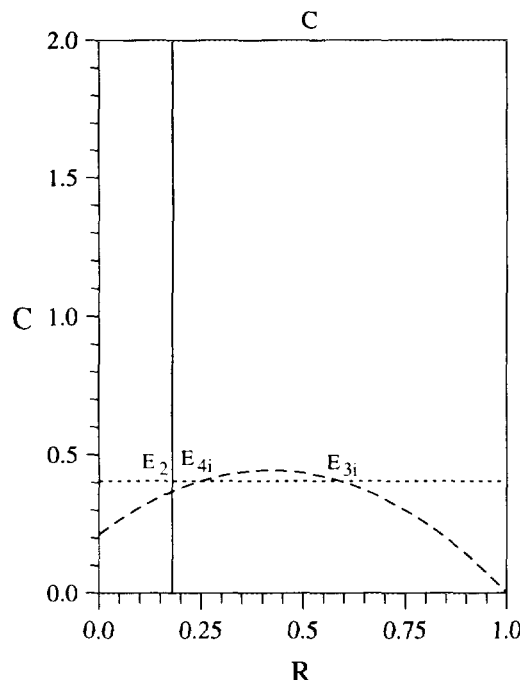
the intersections of which reveal the equilibria structure of the model. We now attempt to reduce the meshing of nullsurfaces in three-dimensional space to a representative form in two dimensions.

Our reduced nullsurface diagrams will be derived from Eqs. (11) to (13) on the $P=0$ plane. In order to understand what the reduced nullsurface diagrams represent we must consider the shape in three-dimensional space of each surface defined by Eqs. (11) to (13). First of all, we note that Eqs. (11) and (13) are independent of P . Because of this the surfaces represented by (11) and (13) will always give the same curves when projected into any constant plane P . A reduction to a representative two-dimensional form is therefore simple since the characteristic shape of both equations occurs on the $P=0$ plane (Fig. 1A). We can consider the positive P axis as rising from the graph straight out of the page. At each P value we get exactly the same two curves represented by (11) and (13) displayed as the dashed and dotted line, respectively, in Fig. 1A. Any intersection of the two curves (11) and (13) in Fig. 1A gives a single point which is representative of a line parallel to the P axis.

We are now left with describing the surface represented by Eq. (12). Does it intersect the line of intersection created by Eqs. (11) and (13)? If it does we have found an equilibrium point. It is evident from Eq. (12) that for any value of C and R , a unique value of P exists. This means that the surface defined by Eq. (12) must necessarily intersect any line of intersection created by Eqs. (11) and (13) once and only once, and thus we know that equilibrium points exist. Our concern is not really with the exact size of the equilibrium P value but rather with the sign. With this in mind we reduce Eq. (12) at $P=0$ and get

$$R = R_0/(y_C - 1), \quad (14)$$





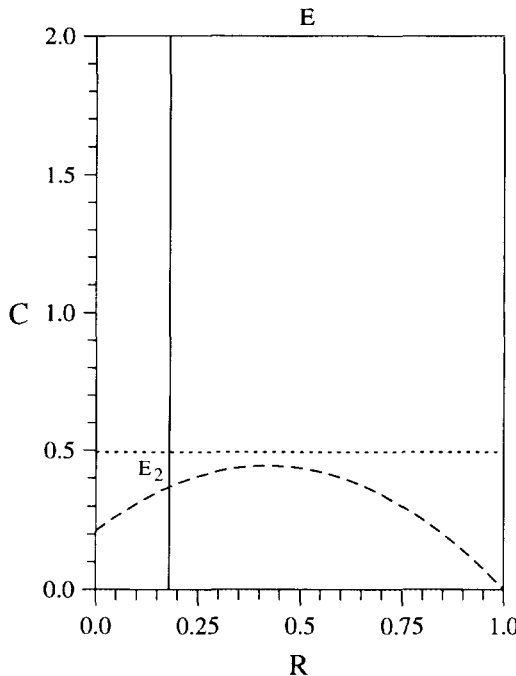


FIG. 1. The reduced nullsurface diagram displaying the curves under the constant parameter setting ($x_C = 0.4$, $x_P = 0.01$, $y_C = 1.9$, $y_P = 3.0$, $R_0 = 0.16$) while we vary the parameter C_0 . Equations (11), (13), and (14) are represented by the dashed, dotted, and solid curves, respectively. E_2 always represents the equilibrium on the CR plane. (A) The diagram at $C_0 = 0.6$, with one interior (E_{3i}) and one exterior (E_{3e}) equilibrium present. (B) $C_0 = 0.735$, and the exterior equilibrium (E_{3e}) has coalesced with the planar equilibrium E_2 . (C) $C_0 = 0.81$, and now two interior equilibria exist (E_{3i}) and (E_{4i}). (D) $C_0 = 0.87$, the two interior equilibria have merged into one now called E_{3i} . (E) $C_0 = 0.987$, no interior equilibria exist.

which we use as the reduced nullsurface curve (solid line) in Fig. 1A. What exactly does this line in the reduced nullsurface diagram mean? We will show that if the intersection point of Eqs. (11) and (13) on the $P = 0$ plane lies to the right of R value determined by Eq. (14), then the value of P given by (12) will be positive, while if the intersection point lies to the left of the R value determined by Eq. (14), we get a negative P value from (12).

If the intersection of (11) and (13) lies to the right of (14) then the R value defined by this intersection is such that

$$R > R_0/(y_C - 1) \quad \text{or equivalently} \quad 1 > y_C R / (R + R_0). \quad (15)$$

If we consider only values of C greater than zero (the ecologically interesting case) then, since all parameters are constrained to being greater than

zero, Eq. (12) must give a positive P value. Similarly, if the intersection of (11) and (13) lies to the left of (14) then Eq. (12) must give a negative P value. Finally, if the intersection of Eqs. (11) and (13) has an R value obeying Eq. (14) then Eq. (12) defines a P value of zero.

Thus, any intersection of (11) and (13) to the right of Eq. (14) represents one and only one interior equilibrium (an equilibrium in the positive octant). Furthermore, any intersection of the reduced nullsurface curves (11) and (13), to the left of the R value given by (14), represents an equilibrium point with a negative P value. Such an equilibrium is ecologically meaningless; however, we make note of it since this information becomes valuable later during the bifurcation analysis. Let us adopt the following notation for equilibria:

E_0 , all trophic levels are collapsed to zero, $(R, C, P) = (0, 0, 0)$, and exist under any parameter setting.

E_1 , only the bottom trophic level exists and therefore the resource reaches carrying capacity, $(1, 0, 0)$, and exists under any parameter setting.

E_2 , the top trophic level is equal to zero, $(a, b, 0)$, where $a = R_0/(y_C - 1)$ and $b = a(1 - a)/x_C$. We require E_2 to always exist ($a < 1$), as the alternative case is trivial. We also note that the C - R plane on which E_2 exists is invariant in system (10). Thus any trajectories on the C - R plane will remain there forever.

E_{3i} , an interior equilibrium to the right of the local maximum of (11) in the reduced nullsurface diagram.

E_{4i} , an interior equilibrium to the left side of the local maximum of (11) in the reduced nullsurface diagram.

E_{4e} , the exterior equilibrium represented by the intersection of (11) and (13) that lies to the right of the local maximum of (11) and to the left of (14).

E_{3e} , the exterior equilibrium represented by the intersection of (11) and (13) that lies to the left of the local maximum of (11) and to the left of (14).

Note that from this reduction it becomes possible to understand the entire equilibrium structure of the model at any point in parameter space. Furthermore, the parametric effect on global equilibria structure can easily be seen from the reduced nullsurface diagrams. For example, consider Figs. 1A-1E. Upon increasing C_0 the line corresponding to (13) moves up until we go from one (E_{3i}^1) to two interior equilibria (E_{3i}^2, E_{4i}^2). Finally, if

we increase C_0 even more we end up in a region of parameter space with no interior equilibria. We have just waked through two local bifurcations which occur at the coalescence of equilibria.

IV. LOCAL BIFURCATION ANALYSIS

Our local bifurcation analysis first considers the codimension one bifurcations and then the higher codimension bifurcations of system (10), identifying bifurcation type by the parametric relationships at the critical values.

IV.1. Codimension 1 Bifurcations

One easy way to search for the simplest codimension one bifurcations of vector fields (transcritical, saddle-node, or pitchfork) is to locate the coalescence of equilibria as we vary a bifurcation parameter. The reduced nullsurface diagram enables us to locate the collision of equilibria and qualify the different types geometrically. Figs. 1A-1C show the collision of a boundary equilibrium (E_2) with an interior equilibrium (E_4) as we vary one bifurcation parameter. We will show that generically any collision with the boundary equilibrium (E_2) that involves either an exterior or interior equilibrium is a transcritical bifurcation. A second qualitatively different simple codimension one bifurcation of system (10) occurs when two interior or two exterior equilibria coalesce Figs. 1C-1E. We will show that this bifurcation is generically a saddle-node bifurcation. Implicit in these qualitative figures of two types of bifurcations is the varying of a bifurcation parameter. Throughout this codimension one bifurcation analysis we do not choose a particular bifurcation parameter. Simply stated, if we reach a critical point in parameter space virtually any parameter in Eqs. (11), (12), or (13) can then be used as the bifurcation parameter. These observations lead to the following two theorems:

THEOREM 1. *In the system (10), a bifurcation takes place at the critical point defined by*

$$C_0 = -R_0(R_0 - y_C + 1)(y_P - 1)/[(x_C(y_C - 1)^2)] \quad (16)$$

$$R_0/(y_C - 1) \neq (1 - R_0)/2. \quad (17)$$

This is always qualitatively the same as a transcritical bifurcation. Fig. 1B shows the qualitative structure of the reduced nullsurface diagram for conditions (16) and (17). See Appendix for proof.

THEOREM 2. *In the system (10), a bifurcation takes place at the critical point defined by*

$$C_0 = (R_0 + 1)^2 (y_p - 1)/(4x_C y_C) \quad (18)$$

$$R_0/(y_C - 1) \neq (1 - R_0)/2. \quad (19)$$

This is always qualitatively the same as a saddle-node bifurcation. Fig. 1D shows the qualitative structure of the reduced nullsurface diagram for conditions (18) and (19). See Appendix for proof.

Dynamical systems theory has shown the existence of parallel codimension one bifurcations for maps or periodic orbits (Guckenheimer and Holmes, 1983). There is no obvious reason for system (10) not to experience codimension one bifurcations of periodic orbits so we must consider the possibility analytically and numerically. We again separate the types of codimension one periodic bifurcations into two parametrically different cases; one, the transcritical case, whenever two cycles coalesce into one at the critical point and rather than collapse, pass through each other merely exchanging stabilities; and two, the cyclic fold (which is analogous to the saddle-node bifurcation of equilibria) where two cycles coalesce and annihilate each other.

THEOREM 3. *In the system (10) any collision of periodic orbits on the boundary plane C - R is generically a transcritical bifurcation of cycles if*

$$R_0/(y_C - 1) \neq (1 - R_0)/2 \quad (20)$$

holds when the two cycles coalesce. See Appendix for proof.

Theorem 3 does not apply, of course, to any collisions of cycles that do not occur on the invariant C - R plane. In this new scenario we have little reason to believe that the cyclic fold (saddle-node) type of bifurcation will not occur as it is the generic case.

So far we have covered codimension one bifurcations that occur when the Jacobian matrix has one and only one simple zero eigenvalue. Another codimension one bifurcation is the Hopf bifurcation which defies this condition. The Hopf bifurcation generically takes place when, at the critical value, a pair of imaginary eigenvalues have zero real parts (Guckenheimer and Holmes, 1983). The Hopf bifurcations of the interior equilibria have been located numerically.

IV.2. On the Existence of Degenerate Bifurcations in System (10)

We are concerned with the possible existence of higher codimension, degenerate bifurcations around interior solutions. Our approach is to

search for higher degeneracies within the linear part of system (10). Two basic possibilities exist in the three-dimensional system (10): one, three-dimensional systems may have multiple real zero eigenvalues; or two, a periodic and steady-state mode interaction arise when a Hopf bifurcation and another codimension one bifurcation occur simultaneously. Theorem 4 determines the existence of a degeneracy in the system (10):

THEOREM 4. *In the system (10) multiple zero real eigenvalues do not exist under any conditions. However, periodic and steady-state bifurcations exist together if and only if the equilibrium under consideration has a P value equal to 0 and*

$$y_C = (1 + R_0)/(1 - R_0) \quad \text{or equivalently} \quad R_0 = (y_C - 1)/(y_C + 1) \quad (21)$$

$$C_0 = \frac{(y_P - 1)[-R_0(R_0 + 1 - y_C)]}{(y_C - 1)^2 x_C} \quad (22)$$

hold. Figure 2 shows the qualitative structure of the reduced nullsurface diagram for conditions (21) and (22). See Appendix for the sketch proof.

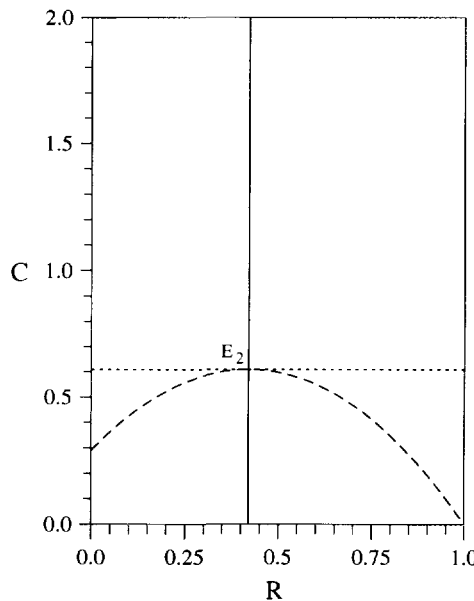


FIG. 2. Reduced nullsurface diagram of the highly degenerate point in system (10). Equations (14), (11), and (13) are represented by the solid, dotted, and dashed curves, respectively. E_2 always represents the equilibrium on the CR plane. Equation (13) is equal to the maximum C value (C_{\max}) attained by Eq. (11). Equation (14) is equal to the R value that gives Eq. (13) its maximum C value (R_{\max}). Parameter values are $x_C = 0.4$, $x_P = 0.01$, $y_C = 1.385$, $y_P = 3.0$, $R_0 = 0.16$, and $C_0 = 1.217$.

VI. QUALITATIVE ANALYSIS AROUND AN ORGANIZING CENTER— THE GLOBAL PICTURE

At this point we are certain of the existence of steady-state and periodic mode interactions in system (10) and can define where in parameter space such degeneracies lie. In the tradition of Thom (1975) we intend to look at two unfolding parameters around these degenerate points defined in Theorem 4. We will analytically and numerically develop curves representing all the local bifurcations as the two unfolding parameters vary around the periodic steady-state mode interaction. This picture becomes an organizing center, as Thom coined it, for system (10) around which we can interpret all the different regions of behaviour. We choose to describe the behaviour around a point close to the chaotic parameter values found by Hastings and Powell (1991). However, one can vary the starting parametric point and find that our organizing center still gives the same topological pattern of regional differences in dynamic behaviour. Thus, these organizing centers exist nearby any parametric setting and act as a focal point for comprehending the whole systems behaviour. We choose to use R_0 and C_0 as the unfolding parameters, as they are easily understood in a biological context. From Table II we see that both R_0 and C_0 are defined in terms of the carrying capacity, K . This implies that varying carrying capacity will vary both unfolding parameters enabling us to comprehend the effects of changing productivity on the dynamical behaviour of system (10). Table III shows the dependent and independent choice of parameter values that give a periodic steady-state mode interaction. The dependent or unfolding parameters have been determined by conditions (21) and (22).

Figure 3 identifies local bifurcations around the degenerate point. All curves present in Fig. 3 have been derived from the previous local

TABLE III
Parameter Values Giving Degenerate Bifurcation

Non-dimensional parameter	Value of parameter
x_C	0.40
x_P	0.01
R_0	0.3353
C_0	2.255
y_C	2.009
y_P	5.0

Note. Where C_0 and R_0 have been determined from conditions (21) and (22) and all other parameters come from Hastings and Powell (1991).

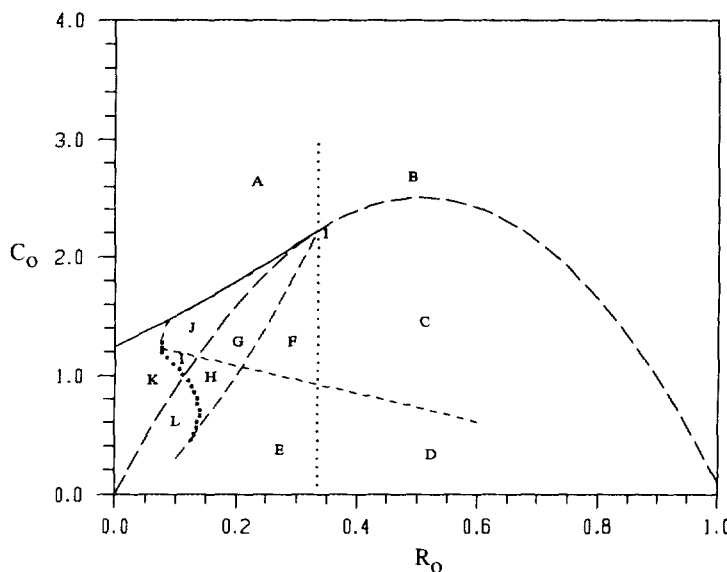


FIG. 3. Local bifurcation curves around the degenerate point found at the parameter set ($x_C = 0.4$, $x_P = 0.01$, $y_C = 2.009$, $y_P = 5.0$). Unfolding parameters are C_0 and R_0 . Cyclic fold curve has been included. The 10 regions are identified by letter. Regions K and L are now also included. The curves displayed are as follows: (—) saddle-node bifurcation curve; (····) transcritical bifurcation curve; (---) transcritical cyclic bifurcation curve; (---) interior Hopf bifurcation curve is the dash-dotted curve; (···) Hopf bifurcation on the C - R plane; and (****) cyclic fold curve. Note that the interior Hopf bifurcation curve continues to the degenerate point (1), as does the cyclic fold curve.

bifurcation theorems except the Hopf bifurcation curves. The planar Hopf curve (made of circles) is determined from condition (21), which is the parametric condition for planar Hopf bifurcations determined by Rosenzweig and MacArthur (1963), while the Hopf bifurcation curve (dash-dotted) for interior equilibrium E_{3i} has been numerically derived. The criticality of the bifurcations has been determined either from the corresponding theorems or from a Hopf bifurcation program (Anfossi, 1991) based on the derivations of Golubitsky and Langford (1981). The occurrence of Hopf bifurcations in system (10) appears numerically always to be supercritical giving rise to a limit cycle. The direction of each bifurcation will be emphasized when we make a pass through all regions in Fig. 3 examining their behaviour. We make one further note: the saddle-node and the interior Hopf bifurcation curves appear to end at the degenerate point. This is actually not the case as they carry on within regions A and B; however, in these regions they involve strictly exterior equilibria and so we chose to ignore them in Fig. 3.

Upon reflection, one thing becomes apparent about the structure of Fig. 3: the degenerate point has a codimension greater than two. It is obvious from the figure that all our local bifurcation curves originate from the same point described by conditions (21) and (22) of Theorem 4. We have uncovered a staggeringly degenerate scenario. Of interest is our subtle misuse of the term “organizing center” which suggests analysis on a codimension equivalent to the degeneracy. We instead offer intuitive results from the perspective of two unfolding parameters while perhaps further research of higher codimension may shed light on some of the global phenomena that this paper only conjectures upon.

There are 12 regions of behaviour currently identified around the degenerate point. Our regional analysis follows the change in phase portrait as we move from region to region. Primary interest is given to interior and boundary regions of phase space; however, at times we will add detail pertaining to exterior regions to clarify the whole bifurcation picture.

Region A. In this region we have a stable planar limit cycle and no interior equilibria. Figure 4A depicts the phase portrait and shows the globally stable nature of the planar limit cycle.

Region B. In this region we have crossed the planar Hopf bifurcation and the stable planar limit cycle disappears leaving a globally stable planar equilibrium (E_2). Figure 4B depicts the qualitative phase structure of this region.

Region C. In this region we have crossed the transcritical bifurcation curve thus changing two things in our interior phase structure. One, the planar equilibrium becomes a saddle of index 1 (E_2) with the repellor in the P direction and two, the bifurcation gives off one stable interior equilibrium (E_{3i}). These changes occur because, as seen from Theorem 4, an exterior saddle equilibrium (E_{4e}) of index 1 coalesces with (E_2) and then returns on the other side of the critical point as a stable interior equilibrium (E_{3i}). Figure 4C depicts the qualitative structure of the phase space. We have a globally stable interior equilibrium (E_{3i}).

Region D. In this region we have moved through an interior supercritical Hopf bifurcation and the behaviour changes only in that the interior equilibrium (E_{3i}) has now become a saddle of index 2, giving off a stable limit cycle. Figure 4D depicts the qualitative structure indicating the global stability of the interior limit cycle.

Region E. In this region we have moved through the planar Hopf bifurcation. Thus the (E_2) equilibrium is now a repellor and a limit cycle exists on the CR plane but is unstable in the P direction (from Theorem 3.2 of Freedman and Waltman, 1977). So we now have a saddle cycle on the plane and a stable cycle in the interior. Figure 4E depicts the qualitative structure of this region and clearly the interior limit cycle is still

globally stable. Note that this region combines two different oscillatory frequencies and dynamics can and will be shown to yield complicated dynamics in the interior.

Region F. In this region we have crossed the interior Hopf bifurcation back to a stable interior equilibrium (E_{3i}). The planar limit cycle remains a saddle cycle repelling in the P direction. Figure 4F depicts the qualitative structure in this region and the (E_{3i}) returns to a globally stable attractor.

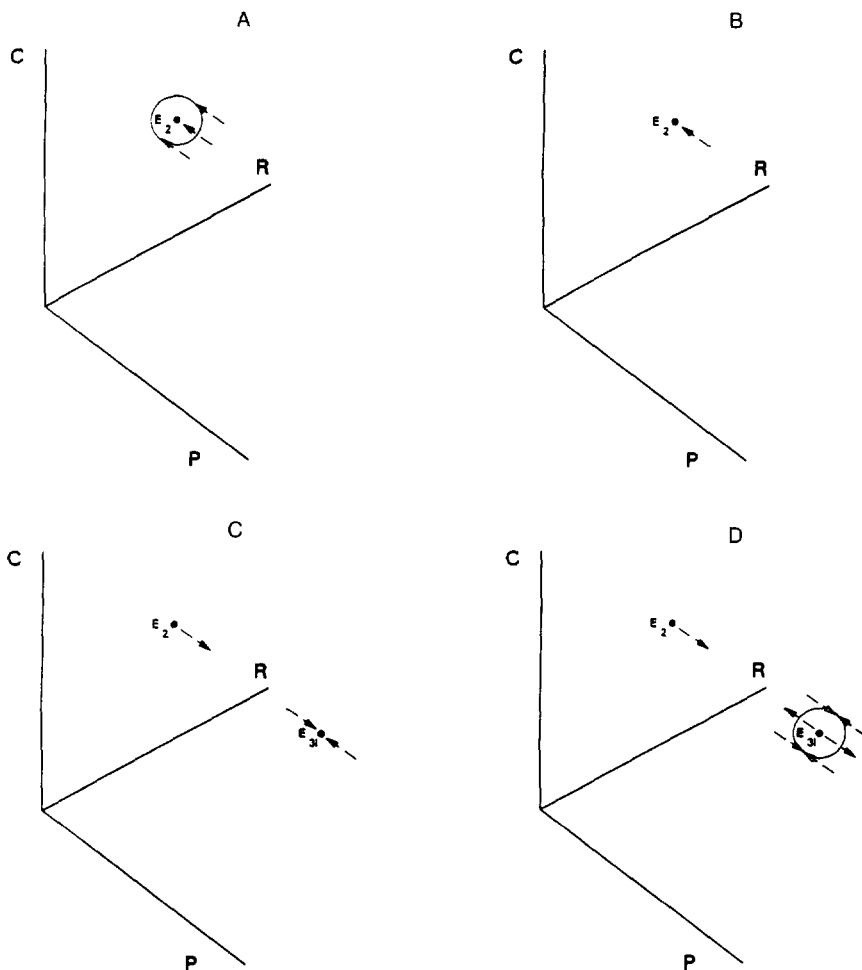


FIG. 4. Diagram displaying basic structure of phase space. Dots represent equilibria, while circles represent invariant sets. Arrows pointing towards an equilibrium or an invariant set represent local stability while arrows going away from an equilibrium or an invariant set represent local instability. Each phase space is thoroughly described in text.

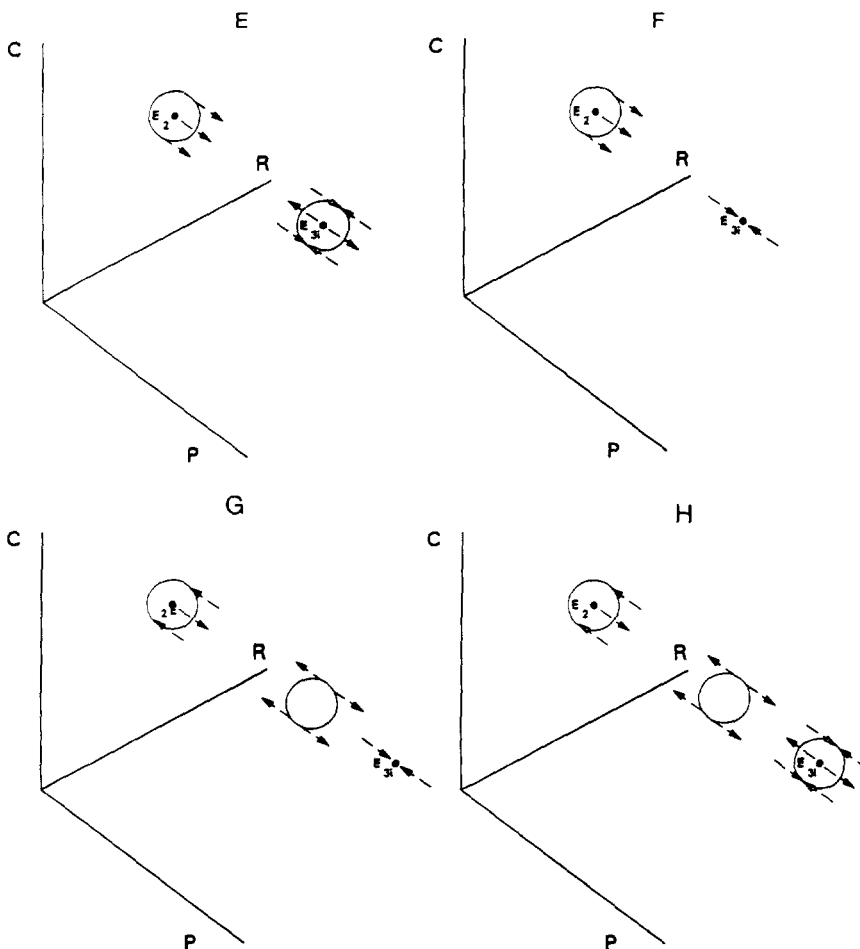


FIG. 4—Continued

Region G. In this region we have crossed a transcritical cyclic bifurcation. This means that the planar saddle cycle is now stable, as is as a new interior saddle cycle that has come from the transcritical bifurcation. Before the transcritical cyclic bifurcation this cycle previously dwelled in the exterior as a stable limit cycle. Where did it come from? It has been numerically determined that it originated in the exterior after a Hopf bifurcation of the exterior equilibrium (E_{3e}). The exterior equilibrium becomes a saddle of index 2 after the transcritical bifurcation. Every trajectory in the exterior collapses to the stable planar limit cycle. With this in mind we show Fig. 4G depicting the qualitative structure in the interior region only.

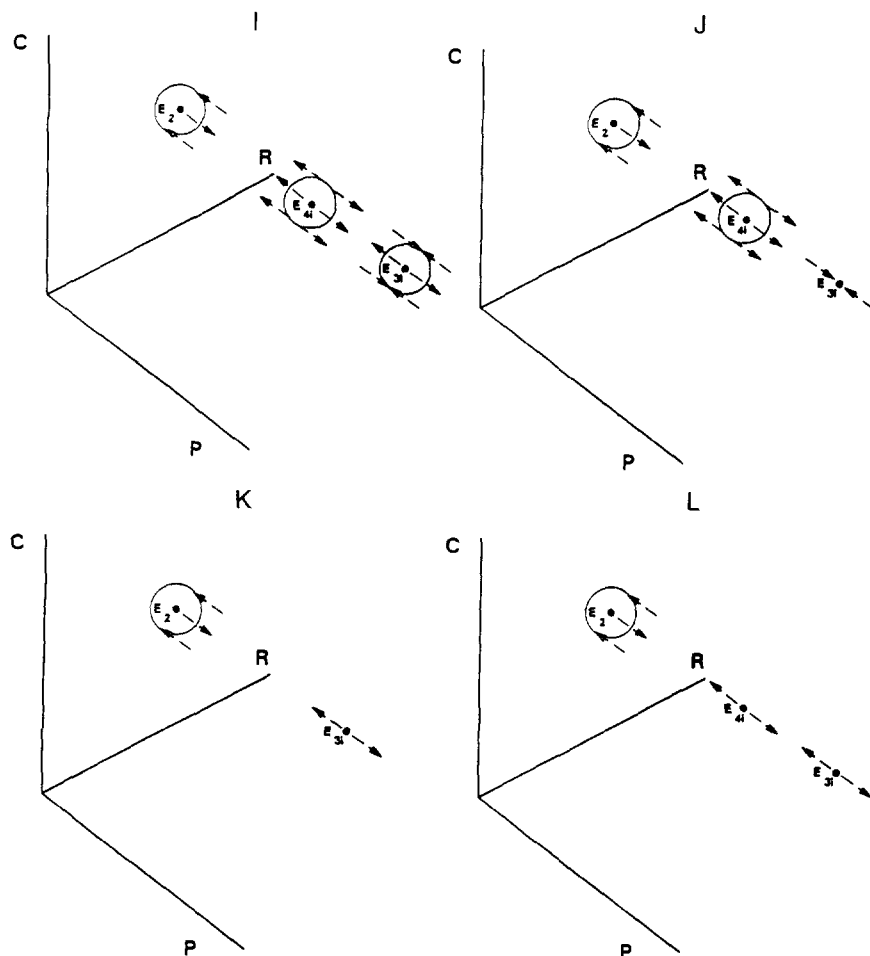


FIG. 4—Continued

Figure 4G shows that the interior saddle cycle now supports a separatrix dividing two basins of attraction. In one basin everything gathers to the stable equilibrium (E_{3i}) while in the other basin every trajectory ends up on the stable planar limit cycle.

Region H. In region H we once again cross the numerically determined Hopf bifurcation curve for the interior equilibrium. Nothing changes from region G except that the interior attractor is now a stable limit cycle. Figure 4H depicts the new phase structure. Once again, we have two frequencies interacting in the interior basin of attraction and thus, complex dynamics can and will arise. The Hastings and Powell (1991) parameter values fall in this region.

Region I. In this region we have crossed the transcritical bifurcation curve. The E_2 equilibrium has now changed from a repellor to an attractor in the P direction. Furthermore, the exterior saddle of index 2 equilibrium previously notated E_{3e} has now reappeared in the interior as a repellor (now notated E_{4i}). This equilibrium, as it earlier spawned the separatrix saddle cycle, can be envisioned as the center and its imaginary eigenvalues give rise to trajectories that act as the spokes, if you will, for the saddle cycle. Figure 4I depicts the phase space structure in this region. Once again, we have two frequencies interacting in the interior basin of attraction and thus, complex dynamics arise.

Region J. In this region we cross the interior Hopf bifurcation curve and thus lose the stable limit cycle as it returns to a stable interior equilibrium (E_{3i}). The planar limit cycle remains stable and the saddle limit cycle continues to act as a separatrix. (E_{4i}) remains connected to the saddle cycle. Figure 4J depicts the new phase space.

In order to pass from region J to region A it is necessary to pass into region I then K first. Passing into region I requires equilibrium E_{3i} to undergo a Hopf bifurcation to a limit cycle. The planar limit cycle remains stable and the saddle cycle continues to act as a separatrix. We have returned to a phase portrait similar to Fig. 4I. In numerical simulations we have discovered the coalescence of the interior saddle cycle and the interior stable cycle followed by the apparent reduction to one basin of attraction, that of the stable planar limit cycle. We have *roughly* depicted this cyclic fold curve by tracking the loss of the interior basin in Fig. 3. For example, as we move through region I towards region A our two interior cycles collide and demolish each other, and then as we pass across the saddle-node curve for interior equilibria we return exactly to the phase portrait described in region A. Let us now describe the last two regions of behaviour, regions K and L.

Region K. Passing from region H into K we realize from reviewing Fig. 4H that both interior cycles are annihilated, leaving us with a stable planar limit cycle and a saddle of index 2 in the interior (E_{3i}). Figure 4K depicts the new phase portrait with the now globally stable planar limit cycle. At the cyclic fold the two frequencies of the once separate cycles merge into one frequency. Any complexities in transient behaviour are due to the action of two incommensurate frequencies.

Region L. Let us first pass from region I into region L. The two interior cycles coalesce, leaving two interior equilibria and a stable planar limit cycle. E_{4i} is a repellor and E_{3i} is a saddle of index 2. Figure 4L depicts the new phase space. Notice that if we pass from K to L by crossing the transcritical bifurcation we simply lose the interior saddle of index 2 in the bifurcation and return to the phase space described by Fig. 4L. At the cyclic

fold the two frequencies of the once separate cycle merge into one frequency. Any complexities in transient behaviour are due to the action of two incommensurate frequencies.

One way to test our local bifurcation analysis is to move through the parameter space defined in Fig. 3 along different paths. If the story told by the local bifurcation curves fits our predicted behaviour as well as numerical results we can begin to feel confident that we have uncovered all the bifurcations of the system (10) near this organizing center. As we described each region and the transition from a previous region we have, in essence, made one such successful walk through the unfolding parameter space. Other paths can be taken and the story predicted remains true to our bifurcation analysis and numerical simulations.

Two further comments are necessary. First, note that we have chosen R_0 and C_0 as unfolding parameters for Fig. 3. This choice of parameters was simply due to the ease in biological interpretation they allow since they are both scaled to the carrying capacity. Changing them both by a constant multiple is identical to manipulating carrying capacity. The choice of any two parameters from the six in system (10) gives a topologically equivalent set of bifurcation curves. Second, if we utilize the biology behind the parameters developed by Yodzis and Innes (1992) we can organize bifurcation curves around a degenerate point that corresponds to plausible biological parameters. McCann and Yodzis (1994a) utilized these tools to show that chaotic dynamics in system (10) were plausible, but occurred only for rather extreme productivities (very high parameter K).

VI.1. *The Existence of Chaos in Regions E, H, and I*

We have numerically identified complex behaviour in three of the regions identified. One thing is common to these regions alone: the existence of two incommensurate frequencies of oscillation in the interior. The bifurcation diagram Fig. 5, produced by plotting successive local minima of the attractor as we vary the parameter x_P , shows the classical period doubling cascade. Certainly, it appears that chaos is likely reached within the thick regions of the bifurcation diagram. Although not a rigorous proof, this lends great plausibility to the case for the existence of chaos in system (10).

Applying the algorithm of Wolf *et al.* (1985), we attempted numerically to calculate the three Lyapunov exponents of the complex dynamics found by Hastings and Powell (1991). Our analysis included 100,000 time units of transient behaviour before the algorithm was applied, followed by 625,000 time units at increments of 1.0 units. We found that one exponent is largely negative (approximately -0.9174) while the other two exponents take on small positive values. (approximately 0.00494 and 0.01424). If this is truly a chaotic attractor then one of the exponents is expected to go to

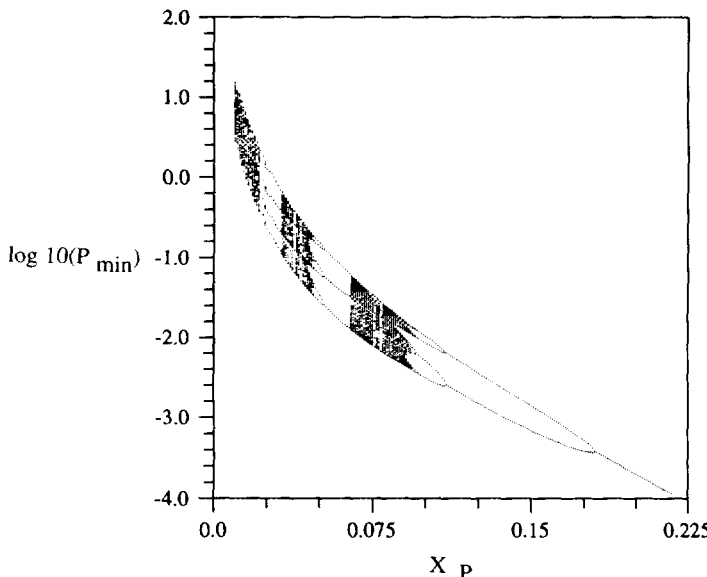


FIG. 5. For a range of values of the parameter x_P , the set of local minima taken on by density in solutions of the system of equations discussed in the text. Other parameters are held constant at $x_C = 0.4$, $y_C = 2.009$, $y_P = 5.0$, $R_0 = 0.333$, $C_0 = 0.5$.

zero while one remains positive; however, if it is simply quasi-periodic behaviour both exponents will fall eventually to zero (Sano and Sawada, 1983). The nature of the exponents is such that chaos seems very likely, yet, probably a weak form of chaos.

VI.2. Routes to Chaos in System (10) and Complex Behaviour in Regions K and L

Let us first consider the routes to chaos found by varying one parameter. As we have already discussed, it seems probable that system (10) undergoes a period-doubling cascade to a chaotic regime (Fig. 5). But are there other routes to chaos? We conjecture, due to the nature of our local bifurcation structure, the existence of a blue sky catastrophe as a route to chaos. We reduced the parameters C_0 and R_0 from the Hastings and Powell parameter range such that our chaotic attractor started in region E , passed through region H gaining an interior saddle cycle, and then ended in region K . Figure 3 shows the path through parameter space that moves the chaotic attractor through the cyclic fold curve. In fact, this is no longer a cyclic fold by definition but rather a form of hysteresis involving a chaotic attractor called the blue sky catastrophe (Rössler, 1976; Grebogi *et al.*, 1983; Abraham and Stewart, 1986). Upon passing the critical point the chaotic attractor is annihilated and we are left with complex transient

behaviour that eventually behaves as described by region K (Fig. 6). McCann and Yodzis (1994b) showed that chaotic transients can give rise to well-bounded long-term oscillations of the food chain in system (10) but which ineluctably and unpredictably lead to the disappearance of the top population, P . This "population disappearance," seemingly random, is entirely deterministic.

As we have mentioned, complex or chaotic behaviour exists in regions involving two cycles. This implies the existence of two incommensurate

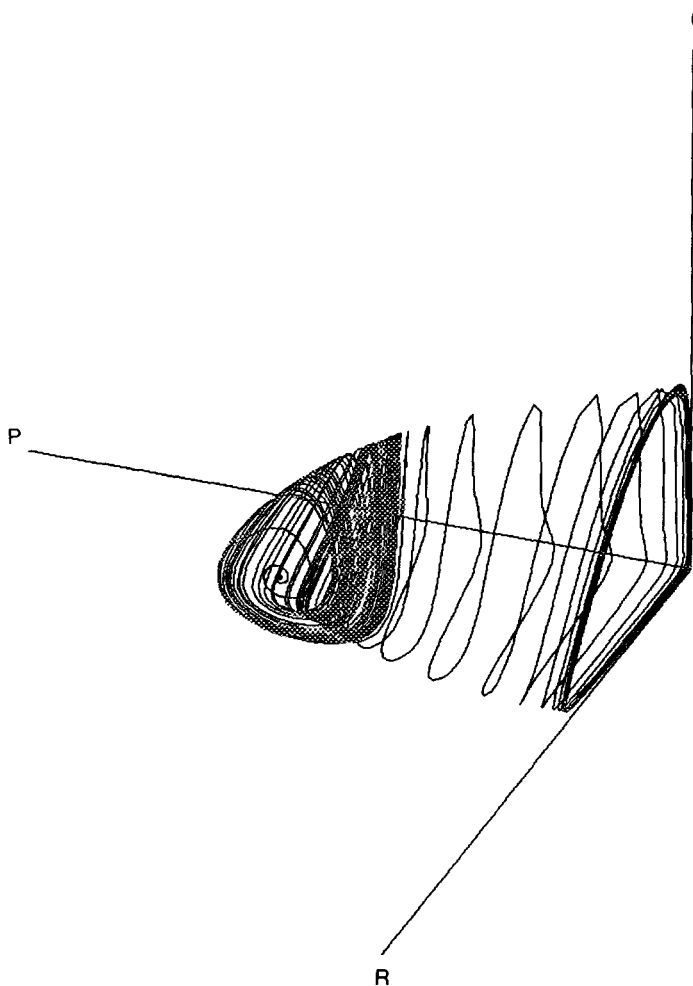


FIG. 6. Transient behavior for the parameter values $x_C = 0.4$, $x_P = 0.08$, $C_0 = 0.5$, $R_0 = 0.16129$, $y_C = 2.876$, $y_P = 5.0$. Transient occurs just after the annihilation of the chaotic attractor due to a blue sky catastrophe.

frequencies and therefore the possibility of the codimension two bifurcation from quasi-periodic to chaotic dynamics. Our system is likely to undergo a transition from attracting invariant torus to chaotic attractor given that we vary two parameters (one for amplitude and one for frequency), such that mode locking is avoided and a route from quasi-periodic to chaotic exists. Due to the difficulty in avoiding mode locking we have been unable to identify a quasi-periodic state in the model (for a thorough explanation of this phenomenon see Arnold, 1965; Herman, 1979). Other investigators (Inoue and Kamifukumoto, 1984) have observed the coexistence of both period doubling and torus to chaos routes within a two-dimensional non-autonomous predator-prey model. We draw attention to this analysis, as they periodically forced the Malthusian rate of prey parameter. This method invokes two competing cycles that are similar in nature to the behaviour we witness in regions E, H, and I.

VII. GLOBAL BIFURCATIONS AND SILNIKOV'S THEOREM

The existence of a blue sky catastrophe has further mathematical repercussions in the context of the system (10). A blue sky catastrophe implies the existence of either a homoclinic or heteroclinic event at the critical point (Thompson and Stewart, 1986). In the sense of the blue sky catastrophe occurring in system (10) the global bifurcation appears as if it is a homoclinic event. If we consider the unstable manifold of a Poincaré section for the saddle cycle before and exactly at the blue sky catastrophe we develop an idea of the complexity of the homoclinic event. Just before the collision of the saddle cycle and the chaotic attractor the unstable manifold of the saddle cycle asymptotically approaches the Poincaré section of the chaotic attractor; however, just at the point of collision the unstable manifold becomes exactly the Poincaré section for the chaotic attractor. Abraham and Stewart (1986) have found and numerically derived the Poincaré sections displaying an extremely similar example of a blue sky catastrophe in the forced Van der Pol oscillator. In three dimensions the homoclinic event is not so easily understood but consists of the complex tangling of saddle inset and outset generating a homoclinic tangle.

We conjecture the existence of at least one other global bifurcation in system (10). Interestingly, the eigenvalues of the E_{3i} equilibrium appear numerically always to fall into the relationship

$$|\lambda_1| > \operatorname{Re} |\lambda_{2,3}|$$

whenever a chaotic attractor exists, where λ_1 is the real eigenvalue and $\lambda_{2,3}$ are the complex eigenvalues. This relationship is the eigenvalue relationship necessary in order to apply Silnikov's theorem (Silnikov, 1965). The question thus arises: Does a homoclinic bifurcation of the equilibrium E_{3i} exist? We have numerically estimated trajectories very close to the one dimensional stable manifold of E_{3i} by moving backward in time from the equilibrium point and relating this trajectory to the interior attractor (Hassard, 1980). By doing this we have numerically witnessed trajectories close to the stable manifold of E_{3i} moving very close to the interior attractor and thus approximating a homoclinic orbit (Fig. 7). Klebanoff and Hastings (1994) have shown, via a reduction to normal form, the existence of a homoclinic event in this system. Finally, it is of interest to note that even if a homoclinic bifurcation is never reached in this scenario but rather the stable manifold comes infinitesimally close to the interior attractor it is possible to develop a corollary of Silnikov's theorem. In this sense the stable and unstable manifold approximate a homoclinic orbit. Holmes (1980) developed a corollary for heteroclinic orbits obeying Silnikov's eigenvalue relationship and a similar method could be developed in this case by mapping the interior attractor to a point and then applying Holmes' corollary of Silnikov's theorem.

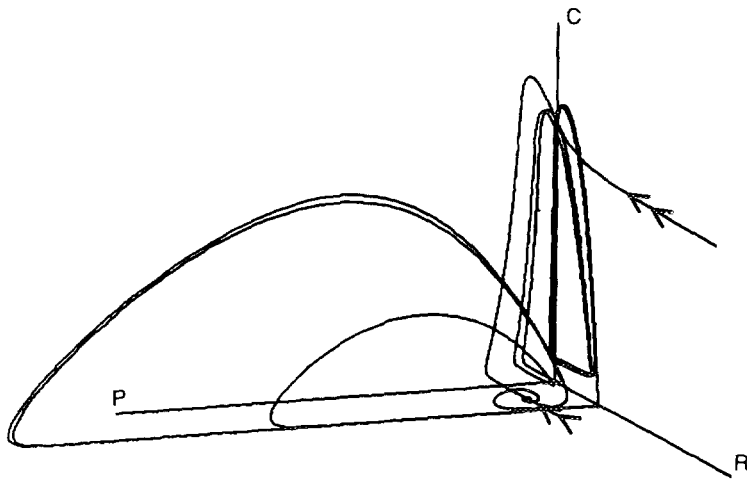


FIG. 7. A numerical estimation of the path of the stable manifold of E_{3i} . The stable manifold shoots in from infinity and follows the strange attractor for a while approximating a homoclinic orbit since the unstable manifold of E_{3i} asymptotically approaches the strange attractor ($x_C = 0.07$, $x_P = 0.01$, $C_0 = 0.05$, $R_0 = 0.16129$, $y_C = 2.009$, $y_P = 5.0$).

VIII. DISCUSSION

This paper has been rather mathematically oriented. Here we synthesize four of the contributions to the ecology of food chain dynamics made by this paper.

First, we have defined a reduced nullsurface diagram that has proven to be a powerful tool for the mathematical analysis of the food chain defined by system (10). It has aided the analysis by giving a simple graphical method for determining when the dynamical behaviour of system (10) changes. We can think of "changes" in the above context—in a loose sense—as at least one equilibrium undergoing a change in local stability. Furthermore, as the reduced nullsurface graphs are simple functions of the system parameters, it is easy to interpret the effect perturbing any parameter will have on the current dynamic behaviour by noting the effects of such a perturbation on the topological structure of the reduced nullsurface diagram. This method is not restricted to type II functional responses in system (10). For example, it would be possible to utilize a reduced nullsurface diagram on system (10) with a type III functional response. It would be interesting to see if the type III functional response will dampen the oscillations sufficiently to avoid complex dynamics.

Second, we have utilized a highly degenerate bifurcation as an organizing center about which the entire behaviours of the system can be unfolded. The mathematical analysis around the highly degenerate point defined in Theorem 4 creates a predictive tool for dynamical behaviour in system (10). The dynamics for any point in parameter space can be predicted by finding the closest point in parameter space to the degeneracy (organizing center) as defined by conditions (21) and (22). The organizing center can be thought of as a point in parameter space in which several types of bifurcations occur simultaneously. If we vary parameters about this point while utilizing the analytical and numerical techniques described in this paper we can unfold all these bifurcations as separate curves in parameter space. Each curve separates regions of qualitatively different dynamical behaviours. Our analysis has unfolded 12 regions of dynamic behaviour that range from stable equilibriums to chaotic transients (Fig. 3). The possible range of dynamic behaviour around any point in parameter space can be determined from the above method and thus we are able to assess not only the local stability but also the global stability of any parameter set.

Third, by embedding the model in empirically derived allometric relationships any of the above complex system behaviours can be deemed plausible or implausible biologically. McCann and Yodzis (1994a, 1994b) have applied the above techniques to assess the plausibility and biological repercussions of complex dynamical behaviour. They have shown that

certain regions of parameter space contain chaotic dynamics that are biologically plausible but that occur only under very high carrying capacities. However, most regions containing chaotic behaviours tend to be either biologically unrealistic or liable to stochastically induced extinction of the top predator (McCann and Yodzis, 1994a). In addition, other biologically plausible parameter sets are associated with population dynamics that are largely dominated by a long and seemingly bounded transient behaviour which suddenly and unpredictably crashes, leaving the top trophic level locally annihilated (McCann and Yodzis, 1994b). This local and rapid population crash is generated entirely from deterministic consumer-resource interactions.

Finally, our analysis has allowed us insight into a possible mechanism for complex dynamic behaviours in highly coupled consumer-resource interactions. We deal here with only three populations or three discrete trophic levels. In either sense our model is a simplification. Our results emphasize the effect oscillating consumer-resource populations can have. Dynamics can and will become complex, even chaotic, when different frequencies mix. The interconnectedness of periodic frequencies, in essence, directs routes to complex behaviour as interactions increase in strength. Undoubtedly, a large ecosystem with a large number of links will, according to our research, include several interacting periodicities and therefore increase the likelihood of complicated dynamics. It seems possible that the dynamic behaviour of a system largely made of stable consumer-resource interactions may be driven by a very few oscillating interactions. With this image in view, it seems odd that any highly coupled consumer-resource system exhibits anything but complex dynamics.

APPENDIX

Proof of Theorem 1. Conditions (16) and (17) qualitatively define the reduced nullsurface for use transcritical bifurcations. Figure 1B shows a reduced nullsurface diagram that obeys these conditions. We will show that a bifurcation occurs that is always qualitatively the same as the transcritical bifurcation whenever a reduced nullsurface diagram obeys these conditions.

In the space of *all* systems of differential equations, the saddle-node bifurcation occurs generically whenever one, and only one, simple eigenvalue attains a zero value. However, particular systems may obey some kind of constraint that enforces genericity on another type of bifurcation. Three necessary conditions (SN1, SN2, SN3 explicated below) have been cited by Guckenheimer and Holmes (1983) for the existence of a saddle-node bifurcation. However, if condition SN2 fails than a transcritical

bifurcation generically takes place; furthermore, if condition SN3 fails as well then a pitchfork bifurcation becomes generic in the system. In order to prove that a transcritical bifurcation takes place it remains to prove that the bifurcation which takes place at (16) and (17) must obey SN1 and SN3 and fails to satisfy SN2 due to some imposed constraint. Our proof analyzes conditions SN1 to SN3 one at a time and finds that SN1 is always satisfied, SN2 always fails, and SN3 generically holds. We show that even if SN3 does not hold, the system (10) still gives a bifurcation with behavior qualitatively the same as that associated with the transcritical bifurcation.

SN1. The requirement is that the Jacobian has a simple eigenvalue 0 and the remaining eigenvalues have either negative or positive real parts at the critical point. It is shown in Theorem 4 that we always have one and only one zero eigenvalue except under the conditions of Theorem 4 which can occur only when (17) is defied.

SN2. The requirement is that

$$w(\partial F/\partial \mu)(\rho, \mu_0) \neq 0,$$

where F is the vector field defined by the right hand side of Eq. (10), ρ is the equilibrium point corresponding to the critical value of the bifurcation parameter (μ_0), and w is the left eigenvector of $DF\mu_0(\rho)$. This condition means that, as we vary the bifurcation parameter in a neighborhood of the critical point, in the generic case (saddle-node) all equilibria involved in the bifurcation disappear on one side of the critical point. System (10) defies this when conditions (16) and (17) are satisfied since it is evident that a trivial equilibrium (E_2) exists in a neighborhood of the critical point (Figs. 1A-1C). E_2 is considered the trivial equilibrium since we can transform it to the origin under the translations

$$\begin{aligned} u &\rightarrow R - a, \quad \text{where } a = R_0/y_C - 1, \\ v &\rightarrow C - a(1 - a)/x_C, \end{aligned}$$

and then make a change of basis such that the center manifold is described by a vector field, F_x , that contains E_2 at the origin. The constraint on system (10) at conditions (16), (17) can now be cast in a simpler format as

$$\begin{aligned} \partial F_x/\partial \mu(o, \mu_0) &= 0, \\ \partial^2 F_x/\partial x \partial \mu(o, \mu_0) &\neq 0, \end{aligned}$$

where F_x is the vector field that defines the center manifold, μ is the bifurcation parameter, o is the equilibrium E_2 translated to the origin, and μ_0

is the value of the bifurcation parameter at the critical point. Essentially this states that a "trivial" equilibrium exists for all values off μ in a neighborhood of the critical point.

SN3. The requirement is that

$$w(\partial^2 F_x / \partial x^2)(\rho, \mu_0) \neq 0,$$

where F is the vector field defined by the right-hand side of the equations in system (10), ρ is the equilibrium at the critical value of the bifurcation parameter (μ_0), and w is the left eigenvector of $DF\mu_0(\rho)$. Under the transformations described above the requirement becomes

$$\partial^2 F_x / \partial x^2(o, \mu_0) \neq 0,$$

where F_x is the vector field that defines the center manifold, μ is the bifurcation parameter, o is the equilibrium E_2 translated to the origin, and μ_0 is the value of the bifurcation parameter at the critical point. We know from the geometry of system (10) that the vector field, F_x , that defines the center manifold must be dominated by an even-powered function since it is easily shown that two equilibria exist on either side of critical point (Figs. 1A and 1C) as we vary a bifurcation parameter,

$$dx/dt = F_x = \mu x - x^{2N},$$

where x is the state variable, μ is the bifurcation parameter, and N is a positive integer. If $N = 1$, SN3 is obeyed. In case $N > 1$, SN3 is not obeyed, but the bifurcation is qualitatively the same as a transcritical. The center manifold has equilibria solutions at $x = 0$ and $\mu = x^{2N-1}$. Whatever the value of N , the bifurcation diagram is qualitatively the same as the transcritical diagram (that is, it has the same topological structure). Q.E.D.

Proof of Theorem 2. Conditions (18) and (19) qualitatively define the reduced nullsurface for saddlenode bifurcations. Figure 1D shows a reduced nullsurface diagram that obeys these conditions. We will show that a bifurcation occurs that is always qualitatively the same as the saddlenode bifurcation whenever a reduced nullsurface diagram obeys these conditions (recall the proof of Theorem 1).

SN1. It is shown in Theorem 4 that we always have one and only one zero eigenvalue except under the conditions of Theorem 4 which can occur only when (19) is defied.

SN2. The generic bifurcation (saddle-node) requires that all equilibria involved in the bifurcation disappear on one side of the critical point. Our geometrical analysis at the condition (18) easily shows that all

equilibria involved disappear on exactly one side of the critical point (Figs. 1C–1E). Thus, the SN2 condition is satisfied.

SN3. Since no equilibrium exists for all values of the bifurcation parameter in a neighbourhood of the critical point and it can be shown that two equilibria coalesce and disappear (Figs. 1C–1E) we know that the center manifold of bifurcations of this type are dominated by even powered terms,

$$dx/dt = \mu - x^{2N},$$

where x is the state variable, μ is the bifurcation parameter, and N is an integer. Once again, if $N = 1$ then SN3 is obeyed. In the case $N > 1$, SN3 is not obeyed, but the bifurcation is qualitatively the same as a saddle-node bifurcation. The center manifold has solutions at $\mu = x^{2N}$. Whatever the value of N , the bifurcation diagram is qualitatively the same as the saddle-node bifurcation diagram. Q.E.D.

Proof of Theorem 3. For cycles, the generic case in the space of all systems is the cyclic fold. However, if one can prove the existence of a cycle involved in the bifurcation that remains intact on both sides of the critical value of the bifurcation parameter, generically, the bifurcation is a trans-critical cyclic bifurcation (Thompson and Stewart, 1986). It remains—to prove Theorem 3—to show that a cycle exists on both sides of the critical point. This is easily seen by recalling Yodzis and Innes (1992), which proves the existence of a stable point or a stable limit cycle in the CR plane. Therefore, if two cycles coalesce at the boundary, the cycle on the CR plane remains when varying the bifurcation parameter in a neighbourhood of the critical value unless a Hopf bifurcation occurs simultaneously (the only bifurcation that takes place on the CR plane (Yodzis and Innes, 1992)). This can occur only at the failure of condition (20). In the system (10), when cycles coalesce exactly at the CR plane the generic bifurcation then becomes the transcritical cyclic bifurcation. Q.E.D.

Sketch proof of Theorem 4. We sketch the outline of the proof here, as the actual proof is exceedingly long and primarily relies on algebraic manipulations. Our proof starts by searching for multiple zero real parts of eigenvalues in the Jacobian of system (10) for R , C , and P greater than zero. After analyzing the Jacobian in the manner of Freedman and Waltman (1977) we are able to show that multiple zero real parts of eigenvalues do not exist under these conditions. We then suppose instead that the equilibrium lies on the CR plane so $P = 0$. The Jacobian now changes, as it is evaluated at E_2 , to

$$\begin{bmatrix} m_{11} & m_{12} & 0 \\ m_{21} & 0 & m_{23} \\ 0 & 0 & m_{33} \end{bmatrix}$$

where

$$m_{11} = 1 - 2R - \frac{x_C y_C C}{R + R_0} \left(1 - \frac{R}{R + R_0} \right)$$

$$m_{12} = -\frac{x_C y_C R}{R + R_0} < 0$$

$$m_{21} = \frac{x_C y_C C}{R + R_0} \left(1 - \frac{R}{R + R_0} \right) > 0$$

$$m_{23} = -\frac{x_P y_P C}{C + C_0} < 0$$

$$m_{33} = -x_P + \frac{x_P y_P C}{C + C_0},$$

and m_{13} , m_{22} , m_{31} , and m_{32} are all equal to zero.

The characteristic equation is

$$g(\lambda) = \lambda^3 + \lambda^2(-m_{33} - m_{11}) + \lambda(m_{33}m_{11} - m_{21}m_{12}) + m_{33}m_{21}m_{12},$$

from which it can be seen that

$$g(0) = m_{33}m_{21}m_{12},$$

and

$$g(m_{33}) = 0,$$

and therefore a simple zero eigenvalue ($\lambda_1 = 0$) exists if and only if $m_{33} = 0$. And $m_{33} = 0$ if and only if

$$C = C_0/(y_P - 1),$$

and since $P = 0$ we know from our reduced nullsurface diagram that C must equal the maximum C value obtainable by Eq. (11), otherwise P will be a nonzero value. Therefore we get condition (22) after substitution and reduction.

If $\lambda_1 = 0$, and therefore $m_{33} = 0$, then the remaining two eigenvalues can be determined from the Jacobian

$$\begin{bmatrix} m_{11} & m_{12} \\ m_{21} & m_{22} \end{bmatrix}$$

and this is exactly the two-dimensional system studied by Yodzis and Innes (1992), who show that there exists a pair of imaginary eigenvalues with zero real parts in this two-dimensional system only when

$$y_C = (1 + R_0)/(1 - R_0).$$

Knowing that $R = R_0/(y_C - 1)$ when $P = 0$, it is easily shown by substituting for y_C that $R = (1 - R_0)/2$. From this we get condition (21). Conditions (21) and (22) define the reduced nullsurface diagram for this case. One, condition (21) forces Eq. (14) to be equal to the R value that gives the maximum C value for Eq. (11). And two, condition (22) forces Eq. (13) to be equal to the maximum C value obtainable by Eq. (11). Thus, the periodic steady-state mode interaction will always appear in a reduced nullsurface diagram qualitatively similar to that shown in Fig. 2.

ACKNOWLEDGMENTS

We thank William Langford for comments on an earlier version of the manuscript. We also thank the National Science and Engineering Research Council for their financial support.

REFERENCES

- ABRAHAM, R. H., AND STEWART H. B. 1986. A chaotic blue sky catastrophe in forced relaxation oscillations, *Physica D* **7**, 181–200.
- ALLEN, J. C. 1990. Chaos and phase locking in predator-prey models in relation to the functional response, *Florida Entomologist* **73**, 100–110.
- ANFOSSI, D. 1991. "Geometry and Dynamics of a Plausible Model for Two Resources and One Consumer," M.Sc. thesis, University of Guelph.
- ARNOLD, V. I. 1965. Small denominators. I. Mappings of the circumference onto itself, *Am. Math. Soc. Transl.* **46**, 213–284.
- FREEDMAN, H. I., AND SO, W. H. 1985. Global stability and persistence of simple food chains, *Math. Biosci.* **76**, 69–86.
- FREEDMAN, H. I., AND WALTMAN, P. 1977. Mathematical analysis of some three-species food chain models, *Math. Biosci.* **33**, 257–276.
- FREEDMAN, H. I., AND WALTMAN, P. 1983. Persistence in models of three interacting predator-prey populations, *Math. Biosci.* **68**, 213–231.
- GARD, T. 1980. Persistence in food webs: Holling-type food chains, *Math. Biosci.* **49**, 61–67.
- GARDINI, L., LUPINI, R., AND MESSIA, M. G. 1989. Hopf bifurcation and transition to chaos in Lotka-Volterra Equations, *J. Theor. Biol.* **145**, 291–305.
- GASPARD, P. 1983. Generation of a countable set of homoclinic flows through bifurcation, *Phys. Lett. A* **97**, 1–4.
- GASPARD, P., AND NICOLIS, G. 1983. What can we learn from homoclinic orbits in chaotic dynamics? *J. Statist. Phys.* **31**, 499–518.
- GIGLIO, M., MUSAZZI, S., AND PERINI, U. 1981. Transition to chaotic behaviour via a reproducible sequence of period-doubling bifurcations, *Phys. Rev. Lett.* **47**, 243–246.

- GOLUBITSKY, M., AND LANGFORD, W. F. 1981. Classification and unfoldings of degenerate Hopf bifurcations, *J. Differential Equations* **41**, 375-415.
- GREBOGI, C., OTT, E., AND YORKE, J. A. 1983. Crises, sudden changes in chaotic attractors, and transient chaos, *Physica D* **7**, 181-200.
- GUCKENHEIMER, J., AND HOLMES, P. 1983. "Nonlinear Oscillations, Dynamical Systems, and Bifurcations of Vector Fields," Springer-Verlag, New York/Berlin/Heidelberg.
- HASSARD, B. D. 1980. Computations of invariant manifolds, in "New Approaches to Nonlinear Problems in Dynamics" (P. J. Holmes, Ed.), pp. 27-42, SIAM, Philadelphia.
- HASTINGS, A., AND POWELL, T. 1991. Chaos in a three-species food chain, *Ecology* **72**, 896-903.
- HERMAN, M. R. 1979. Sur la conjugaison différentiable des difféomorphismes du cercle à des rotations, *Publ. Math. IHES* **49**, 5-233.
- HOLLING, C. S. 1959. Compensation in mammal predation of the European pine sawfly, *Can. Entomologist* **91**, 293-318.
- HOLMES, P. J. 1980. Unfolding a degenerate nonlinear oscillator: A codimension two bifurcation, *Ann. N.Y. Acad. Sci.* **357**, 473-488.
- INOUE, M., AND KAMIFUKUMOTO, H. 1984. Scenarios leading to chaos in a forced Lotka-Volterra model, *Progr. Theor. Phys.* **71**, 930-937.
- KLEBANOFF, A., AND HASTINGS, A. 1994. Chaos in a three-species food chain, *J. Math. Biol.* **32**, 427-451.
- LOTKA, A. J. 1925. "Elements of Physical Biology," Williams and Wilkins, Baltimore.
- MCCANN, K., AND YODZIS, P. 1994a. Biological conditions for chaos in a three species food chain, *Ecology* **75**, 561-564.
- MCCANN, K., AND YODZIS, P. 1994b. Nonlinear dynamics and population disappearances, *Am. Nat.* **144**, 863-869.
- RESCIGNO, A., AND JONES, K. G. 1972. The struggle for life. 3. A predator-prey chain, *Bull. Biophys.* **34**, 521-532.
- ROSENZWEIG, M. 1973. Exploitation in three trophic levels, *Am. Nat.* **107**, 275-294.
- ROSENZWEIG, M. L., AND MACARTHUR, R. H. 1963. Graphical representation and stability conditions of predator-prey interactions, *Am. Nat.* **97**, 209-220.
- RÖSSLER, O. E., 1976. Different types of chaos in two simple differential equations, *Z. Naturforsch* **31a**, 1664-1670.
- SANO, M., AND SAWADA, P. 1983. Transition from quasi-periodicity to chaos in a system of coupled non-linear oscillators, *Phys. Lett. A* **97**, 73-76.
- SCHAFFER, W. M., AND KOT, M. 1985. Do strange attractors govern ecological systems? *BioScience* **35**, 342-350.
- SIGGIA, E. D. 1983. A universal transition from quasi-periodicity to chaos, *Physica D* **7**, 302.
- SILNIKOV, L. P. 1965. A case of the existence of a denumerable set of periodic motions, *Soviet Math. Dokl.* **6**, 163-166.
- THOM, R. 1975. "Structural Stability and Morphogenesis," Benjamin, Reading, MA.
- THOMPSON, J. M. T., AND STEWART, H. B. 1986. "Nonlinear Dynamics and Chaos," Wiley, New York.
- TILMAN, D. 1986. A consumer-resource approach to community structure, *American Zoologist* **26**, 5-22.
- VANDERMEER, J. 1991. Contributions to the global analysis of 3-D Lotka-Volterra equations: Dynamic boundedness and indirect interactions in the case of one predator and two prey, *J. Theor. Biol.* **148**, 545-561.
- VEZINA, A. F. 1985. Empirical relationships between predator and prey size among terrestrial vertebrate predators, *Oecologia* **67**, 555-565.
- VOLTERRA, V. 1926. Variations and fluctuations of the numbers of individuals in animal species living together. (Reprinted in 1931, "Animal Ecology" (R. N. Chapman, Ed.), McGraw-Hill, New York.)

- WOLF, A., SWIFT, J. B., SWINNEY, H. L., AND VASTANO, J. A., 1985. Determining Lyapunov exponents from a time series, *Physica* **16**, 285-317.
- YODZIS, P. 1994. The trophodynamics of whole ecological communities, in "Frontiers in Mathematical Biology," Lecture Notes in Biomathematics (S. A. Levin, Ed.), pp. 443-453, Springer-Verlag, New York.
- YODZIS, P., AND INNES, S. 1992. Body Size and consumer-resource dynamics, *Am. Nat.* **139**, 1151-1175.